Novel One-Dimensional Organic−Inorganic Polyoxometalate Hybrids Constructed from Heteropolymolybdate Units and Copper−Aminoacid Complexes
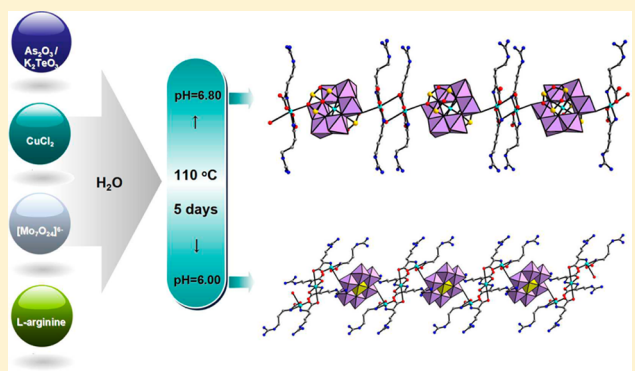
Jun-Wei Zhao,*[,†,‡] Jing-Li Zhang,[†] Yan-Zhou Li,[†] Jing Cao,[†] and Li-Juan Chen*[,†]

[†]Institute of Molecular and Crystal Engineering, Henan Key Laboratory of Polyoxometalate Chemistry, College of Chemistry and Chemical Engineering, Henan University, Kaifeng, Henan 475004, People's Republic of China

[‡]State Key Laboratory of Structural Chemistry, Fujian Institute of Research on the Structure of Matter, Chinese Academy of Sciences, Fuzhou, Fujian 350002, People's Republic of China

S *Supporting Information*

ABSTRACT: Two unique organic−inorganic hybrid heteropolymolybdates with copper−aminoacid complexes $[Cu(arg)_2]_2[(CuO_6)Mo_6O_{18}(As_3O_3)_2]\cdot 4\ H_2O$ (**1**) and $[Cu(arg)_2]_3[TeMo_6O_{24}]\cdot 8H_2O$ (**2**) (arg = L-arginine) have been prepared under the 110 °C hydrothermal environments and structurally characterized by elemental analyses, IR spectra, thermogravimetric (TG) analyses, and single-crystal X-ray diffraction. **1** stands for the first one-dimensional (1D) chain organic−inorganic hybrid arsenomolybdate constructed from lantern-shaped $[(CuO_6)Mo_6O_{18}(As_3O_3)_2]^{4−}$ units through dinuclear $[Cu_2(arg)_4]^{4+}$ connectors, whereas **2** represents an unprecedented 1D chain organic−inorganic hybrid telluromolybdate built by Anderson-type $[TeMo_6O_{24}]^{6−}$ fragments via trinuclear $[Cu_3(arg)_6]^{6+}$ bridges. Variable-temperature magnetic susceptibilities of **1** and **2** have been investigated and both illustrate the weak antiferromagnetic coupling within copper centers mediated by the carboxyl groups of arg ligands. Moreover, the solid-state electrochemical and electrocatalytic properties of **1** have been carried out in 1 mol $L^{−1}$ H_2SO_4 aqueous solution by entrapping it in a carbon paste electrode. **1** displays apparent electrocatalytic activities toward the reduction of nitrite and bromate.

INTRODUCTION

Since the era of Berzelius, polyoxometalates (POMs), as a versatile family of metal−oxygen clusters with oxygen-rich surfaces and controllable sizes, shapes, and compositions, have become one of the highest-growing domains in inorganic chemistry and attracted persistent interest due not only to their structural aesthetics and unmatched diversities but also to their tunable range of physical and chemical properties in catalysis, material science, photochemistry, and electrochemistry.[1] In the past two decades, framing and generation of novel organic−inorganic hybrid POM-based materials with neoteric structures and value-added properties have been an attractive and challenging mission in modern inorganic chemistry and material chemistry. In such respect, a large number of unique organic−inorganic hybrid heteropolytungstates constructed from various POM units and transition-metal (TM)−organic cations have been extensively reported.[2] Moreover, such many hybrids display special functionalities for some certain fields. For example, Duan et al. discovered the chiral POM-based hybrid metal−organic framework materials by incorporating the oxidation catalyst $[\alpha\text{-}BW_{12}O_{40}]^{5−}$ and the chiral L- or D-pyrrolidin-2-ylimidazole into one single framework, which show the asymmetric dihydrox-

ylation of olefins with excellent stereoselectivity.[2b] Mizuno's group reported an ionic crystal $K_2[Cr_3O(OOCC_2H_5)_6(H_2O)_3]_2[\alpha\text{-}SiW_{12}O_{40}]\cdot 3H_2O$ with hydrophilic and hydrophobic channels in the crystal lattice and investigated its amphiphilic guest sorption performance.[2g] Although polyoxomolybdates are also an important subclass in POM chemistry, reports on organic−inorganic hybrids based on heteropolymolybdate (HPM) building blocks and TM−organic complexes are limited,[3] which are principally related to the lower chemical stability of polyoxomolybdates in aqueous solution than polyoxotungstates. However, synthesis and exploration on HPM-based organic−inorganic hybrid materials with TM−aminoacid complexes are only in their infancy,[4a] albeit several HPMs with covalently bound amino acids have been reported.[4b,c] With the profound development of POM chemistry and the urgent requirement of science and technology, the exploration and assembly of organic−inorganic hybrid multicomponent HPMs decorated by TM−aminoacid complexes

have been developed as an emerging and challenging area. Apparently, the appropriate option of aminoacid ligands is undoubtedly a key factor in assembling of HPM/TM/aminoacid organic−inorganic hybrids. As our continuous goal in searching for novel organic−inorganic hybrid POMs with the strategy of employing TM coordination complexes as charge compensation cations, decorative groups, and bridging linkers,[3b,5] recently, we have launched research on reactions of polyoxomolybdate precursors, subvalent lone-electron pairs containing $As^{III}/Se^{IV}/Te^{IV}$ elements with TM cations in the presence of aminoacid ligands. In the present contribution, $(NH_4)_6Mo_7O_{24}\cdot4H_2O$, $As_2O_3/K_2TeO_3/Na_2TeO_3$, $CuCl_2\cdot2H_2O$, and L-arginine (arg) were selected based on the following reasons: (1) the lone-electron pair containing $As^{III}/Se^{IV}/Te^{IV}$ elements can be easily combined with molybdates generating various HPM fragments; furthermore, in contrast to the tetrahedrally coordinated heteroatoms $P^V/As^V/Si^{IV}/Ge^{IV}$, the stereochemical effect of the lone-electron pairs located on top of the trigonal pyramids of $As^{III}/Se^{IV}/Te^{IV}$ elements can to some extent prevent the formation of closed HPM cage structures,[6] thus reducing the steric hindrance of HPMs combining with Cu−arg complexes; (2) flexible coordination geometries (trigonal bipyramid, square pyramid, and octahedron) of copper cations are beneficial to react with labile HPM segments to create novel organic−inorganic hybrid multicomponent HPMs and the Jahn−Teller effect of the octahedron and pseudo-Jahn−Teller effect of the square pyramid for copper cations can also overcome larger steric hindrance and help to stabilize the outcomes;[7] (3) L-arginine has flexible side chains and carboxyl and amino coordination sites (Scheme S1 of the Supporting Information), which allows it to conform to the coordination environments of copper ions and can function as excellent ligands to merge copper centers, giving rise to interesting architecture and further tuning the relationship between structures and properties. With these ideas in mind, we have extensively performed many experiments. Eventually, two unique organic−inorganic hybrid HPTs with copper−arg complexes $[Cu(arg)_2]_2$ $[(CuO_6)Mo_6O_{18}(As_3O_3)_2]\cdot4H_2O$ (**1**) and $[Cu(arg)_2]_3[TeMo_6O_{24}]\cdot8H_2O$ (**2**) have been synthesized under 110 °C hydrothermal environments. Single-crystal structural analyses indicate that **1** is an organic−inorganic hybrid one-dimensional (1D) extended chain made up of lantern-shaped $[(CuO_6)Mo_6O_{18}(As_3O_3)_2]^{4-}$ arsenomolybdate units through dinuclear $[Cu_2(arg)_4]^{4+}$ connectors, whereas **2** is an organic−inorganic hybrid 1D-extended chain telluromolybdate formed by disc Anderson-type $[TeMo_6O_{24}]^{6-}$ subunits via trinuclear $[Cu_3(arg)_6]^{6+}$ bridges. Moreover, the magnetic susceptibilities of **1** and **2** have been investigated. The solid-state electrochemical and electro-catalytic properties of **1** have been carried out in 1 mol L^{-1} H$_2$SO$_4$ aqueous solution by entrapping it in a carbon paste electrode (CPE). **1**-CPE was employed to electro-catalyze the reduction of nitrite and bromate. The results show that **1**-CPE exhibits the apparent electro-catalytic activities toward the reduction of nitrite and bromate.

■ EXPERIMENTAL SECTION

Materials and Methods. All chemicals were commercially purchased and used without further purification. C, H, and N elemental analyses were carried out on a Perkin−Elmer 2400−II CHNS/O analyzer. IR spectra were recorded from solid samples palletized with KBr on a Nicolet 170 SXFT−IR spectrometer in the range of 400−4000 cm^{-1}. Inductively coupled plasma atomic emission spectrometry (ICP-AES) was performed on a Perkin-Elmer Optima 2000 ICP-AES

spectrometer. TG analyses were performed under air atmosphere on a Mettler−Toledo TGA/SDTA 851^e instrument with a heating rate of 10 °C min^{-1} from 25 to 800 °C. Magnetic measurements were conducted on a Quantum Design MPMS XL-7 magnetometer in the temperature range of 2−300 K. Magnetic susceptibility data were corrected from the diamagnetic contributions as deduced by using Pascal's constant tables. Cyclic voltammograms were recorded on a CS electrochemical workstation (Wuhan Corrtest Instrument Company LTD) at room temperature. A conventional three-electrode system was used. Platinum gauze was used as a counter electrode, and an Ag/AgCl electrode was referenced. Chemically bulk-modified carbon paste electrodes (CPEs) were used as working electrodes.

Synthesis of $[Cu(arg)_2]_2[(CuO_6)Mo_6O_{18}(As_3O_3)_2]\cdot4H_2O$ (1). A mixture of As$_2$O$_3$ (0.158 g, 0.799 mmol), CuCl$_2$·2H$_2$O (0.085 g, 0.499 mmol), (NH$_4$)$_6$Mo$_7$O$_{24}$·4H$_2$O (0.405 g, 0.328 mmol), arg (0.053 g, 0.304 mmol), and H$_2$O (8 mL) were stirred for 2 h. The pH value of the mixture was carefully adjusted with a dilute NaOH solution (2 mol L^{-1}) to approximately 6.80 and then sealed in a 25 mL Teflon-lined steel autoclave kept at 110 °C for 5 days and then cooled to room temperature. Blue prismatic crystals were obtained by filtering, washed with distilled water, and dried in air at ambient temperature. Yield: ca. 32% based on arg. Anal. Calcd (%) for C$_{24}$H$_{64}$As$_6$Cu$_3$Mo$_6$N$_{16}$O$_{42}$: C, 11.70; H, 2.62; N, 9.09; Cu, 7.73; As, 18.24; Mo, 23.36. Found: C, 11.86; H, 2.77; N, 8.92; Cu, 7.55; As, 18.38; Mo, 23.52. IR (KBr, cm^{-1}): 3457(s), 3144(s), 3053(w), 2836(w), 1677(s), 1624(s), 1431(s), 1393(w), 932(s), 887(s), 782(s), 645(s), 567(m), 457 (w).

Synthesis of $[Cu(arg)_2]_3[TeMo_6O_{24}]\cdot8H_2O$ (2). K$_2$TeO$_3$ (0.208 g, 0.820 mmol), CuCl$_2$·2H$_2$O (0.119 g, 0.698 mmol), (NH$_4$)$_6$Mo$_7$O$_{24}$·4 H$_2$O (0.407 g, 0.329 mmol), and arg (0.061 g, 0.399 mmol) were suspended in H$_2$O (8 mL). The mixture was stirred for 2 h; its pH value was carefully adjusted with a dilute NaOH solution (2 mol L^{-1}) to approximately 6.00, sealed in a 25 mL Teflon-lined steel autoclave, kept at 110 °C for 5 days, and then cooled to room temperature. Blue prismatic crystals were obtained by filtering, washed with distilled water, and dried in air at ambient temperature. Yield: ca. 28% based on arg. Anal. Calcd (%) for C$_{36}$H$_{100}$Cu$_3$Mo$_6$N$_{24}$O$_{44}$Te: C, 17.53; H, 4.09; N, 13.63; Cu, 7.73; Te, 5.17; Mo, 23.33. Found: C, 17.68; H, 4.22; N, 13.52; Cu, 7.66; Te, 5.30; Mo, 23.22. IR (KBr, cm^{-1}): 3433(s), 3353(s), 3269 (s), 3168(s), 3081(s), 2863(w), 1650(s), 1608(s), 1450(w), 1380 (m), 1323(w), 1138(m), 917(s), 890(s), 807(m), 676(s), 612(s), 555 (w).

Preparations of 1-CPE. 1-CPE was fabricated as follows: 30 mg of graphite powder and 10 mg of **1** were mixed and ground together by an agate mortar and pestle to achieve a uniform mixture, and then 0.05 mL of paraffin oil was added with stirring. The homogenized mixture was packed into a glass tube with a 3.0 mm inner diameter, and the tube surface was wiped with paper. Electrical contact was established with a Cu rod through the back of the electrode.

X-ray Crystallography. Single-crystal X-ray diffraction data for **1** and **2** were collected on a Bruker APEX−II CCD detector at 296(2) K with Mo Kα radiation (λ = 0.71073 Å). Direct methods were used to solve their structures and to locate the heavy atoms using SHELXTL−97.[8] The remaining nonhydrogen atoms were found from successive difference Fourier syntheses and full-matrix least-squares refinements on F^2. Lorentz polarization and empirical absorption corrections were applied. All the nonhydrogen atoms were anisotropically refined, except for some water molecules and oxygen and carbon atoms. The positions of hydrogen atoms attached to carbon and nitrogen atoms were geometrically placed. All hydrogen atoms were refined isotropically as a riding model using the default SHELXTL parameters. The hydrogen atoms associated with the water molecules were not located from the difference Fourier maps. The detailed crystallographic data and structure refinement parameters for **1** and **2** are summarized in Table 1. Crystallographic data for the structures reported in this paper have been deposited in the Cambridge Crystallographic Data Centre with CCDC 935823 and 978422 for **1** and **2**, respectively.

■ RESULTS AND DISCUSSION

Synthesis. **1** and **2** were obtained by reaction of $(NH_4)_6Mo_7O_{24}\cdot4H_2O$ with As_2O_3/K_2TeO_3, $CuCl_2\cdot2H_2O$ in

Table 1. X-ray Diffraction Crystallographic Data for 1 and 2

|	1	2
empirical formula	$C_{24}H_{64}As_6Cu_3Mo_6N_{16}O_{42}$	$C_{36}H_{100}Cu_3Mo_6N_{24}O_{44}Te$
formula weight	2464.72	2467.29
crystal system	triclinic	triclinic
space group	$P\bar{1}$	$P\bar{1}$
a (Å)	10.3413(13)	10.9476(9)
b (Å)	11.9522(16)	11.3888(9)
c (Å)	13.6997(17)	16.2334(13)
α (deg)	104.168(2)	89.3290(10)
β (deg)	96.189(2)	78.6080(10)
γ (deg)	95.169(2)	82.3830(10)
V (Å^{-3})	1620.3(4)	1966.4(3)
Z	1	1
μ (mm^{-1})	5.237	2.191
$F(000)$	1192	1227
T (K)	296(2)	296(2)
limiting indices	$-12 \leq h \leq 12$	$-11 \leq h \leq 13$
	$-13 \leq k \leq 14$	$-13 \leq k \leq 13$
	$-10 \leq l \leq 16$	$-19 \leq l \leq 18$
no. of reflections collected	8296	9972
no. of independent reflections	5661	6849
R_{int}	0.0269	0.0124
data/restraints/ parameters	5661/8/343	6849/7/507
goodness-of-fit on F^2	1.089	1.028
final R indices $[I > 2\sigma(I)]$	$R_1 = 0.0576$	$R_1 = 0.0377$
	$wR_2 = 0.1554$	$wR_2 = 0.0931$
R indices (all data)	$R_1 = 0.0678$	$R_1 = 0.0472$
	$wR_2 = 0.1596$	$wR_2 = 0.0979$

the presence of L-arginine under 110 °C hydrothermal conditions. Recently, although the $(NH_4)_6Mo_7O_{24}\cdot 4H_2O$ precursor has been intensively utilized in the construction of TM-substituted polyoxomolybdates,[9a–d] little attraction is performed on the system including $(NH_4)_6Mo_7O_{24}\cdot 4H_2O$, subvalent lone-electron pair containing $As^{III}/Se^{IV}/Te^{IV}$ components, TM cations, and amino acid ligands. In consideration of the structural diversities of molybdenum-oxo clusters, the stereochemical effect of lone-electron pairs located on top of the trigonal pyramids of the $As^{III}/Se^{IV}/Te^{IV}$ elements, the various coordination modes, and the Jahn–Teller effect of Cu^{II} ions, coordination flexibility of amino acids with the variety of side chains, and the merits of the hydrothermal reaction, the system including $(NH_4)_6Mo_7O_{24}\cdot 4H_2O$, $As^{III}/Se^{IV}/Te^{IV}$ elements, Cu^{II} cations, and arg was first of all developed. When As_2O_3 was utilized in this system, an organic–inorganic hybrid HPT with copper–arg complexes $[Cu(arg)_2]_2[(CuO_6)Mo_6O_{18}(As_3O_3)_2]\cdot 4H_2O$ (**1**) was first obtained, which shows a 1D chain fashion constructed from lantern-shaped $[(CuO_6)Mo_6O_{18}(As_3O_3)_2]^{4-}$ arsenomolybdate units via dinuclear $[Cu_2(arg)_4]^{4+}$ linkers. When K_2TeO_3 was used, an organic–inorganic hybrid $[Cu(arg)_2]_3[TeMo_6O_{24}]\cdot 8H_2O$ (**2**) was consecutively isolated, which also illustrates a 1D infinitely extended chain architecture built by Anderson-type $[TeMo_6O_{24}]^{6-}$ telluromolybdate units by trinuclear $[Cu_3(arg)_6]^{6+}$ connectors. When Na_2SeO_3 replaced K_2TeO_3, unexpectedly, a previous reported inorganic three-dimensional (3D) selenate $CuSeO_3\cdot 2H_2O$ was made,[9e] in which

$\{CuO_5\}$ square pyramids and $\{SeO_3\}$ trigonal pyramids were interconnected. Moreover, we tried our best to use Sb_2O_3 and Bi_2O_3, respectively, substituting for As_2O_3 under similar conditions to prepare analogous HPM/Cu/arg hybrids, but finally, we failed. These experimental results manifest that different subvalent lone-electron-pair-containing elements have distinct reaction activities in this system and have diverse effects on the formation, crystal growth, and structures of the final product phases. As we know, the pH value also is a crucial factor in the hydrothermal system and can greatly influence the crystallization and structural construction of the products. As a result, the influence of the pH value on this system has been investigated. Research results indicate that **1** and **2** can be made in the pH region between 5.5 and 7. When the pH value is lower than 5.5 or higher than 7, **1** and **2** cannot be afforded, which suggest that the pH value plays a key role in the formation and construction of structures under the studied system. It should be pointed out that the left-handed arginine was successfully introduced into **1** and **2**, but the chirality on the carbon atoms did not transfer to the structures of **1** and **2** and only racemic products were obtained, probably because the in situ formation of the centrosymmetric HPM subunits $[(CuO_6)Mo_6O_{18}(As_3O_3)_2]^{4-}$ in **1** and $[TeMo_6O_{24}]^{6-}$ in **2** induced the symmetric distribution of $[Cu(arg)_2]^{2+}$ cations on both sides of heteropolymolybdate subunits, resulting in the loss of chirality. This phenomenon was encountered in the previous studies in the field of POMs.[4b,10a]

IR Spectra. IR spectra for **1**, **2**, $(NH_4)_6Mo_7O_{24}\cdot 4H_2O$, and L-arginine were recorded as KBr pellets in the range of 4000−400 cm^{-1} (Figure S1 of the Supporting Information). For **1**, three groups of characteristic vibration absorption bands are observed at 932, 887; 782; and 645 cm^{-1}, which are attributed to the $\nu(Mo-O_t)$, $\nu(As-O)$, and $\nu(Mo-O_b)$ bonds, respectively.[3h,9a] With regard to **2**, three groups of characteristic vibration bands at 917, 890; 807; and 676(s), 612(s) cm^{-1} are respectively assigned to the $\nu(Mo-O_t)$, $\nu(Te-O)$, and $\nu(Mo-O_b)$ bonds.[9f] The signals appearing at 3144 and 2836 cm^{-1} for **1** and 3168 and 2863 cm^{-1} for **2** are attributable to the $\nu(NH_2)$ and $\nu(CH_2)$ stretching vibrations, while the resonances centered at 1624 and 1393 cm^{-1} for **1** and 1608 and 1380 cm^{-1} for **2** are assigned to the $\delta(NH_2)$ and $\delta(CH_2)$ bending vibration, respectively. As a rule, the carboxylic group is anticipated to supply rather intense absorption bands from the asymmetric and symmetric stretching vibrations.[10b,c] Thus, the strong absorption band at 1677 cm^{-1} in **1** and 1650 cm^{-1} in **2** is assigned to the asymmetric stretching vibration of the carboxylic group [denoted as $\nu_{asym}(CO_2^-)$], while the absorption band at 1431 cm^{-1} in **1** and 1450 cm^{-1} in **2** is ascribed to the symmetric stretching vibration of the carboxylic group [denoted as $\nu_{sy}(CO_2^-)$]. Furthermore, the separation $(\Delta\nu)$ between $\nu_{asym}(CO_2^-)$ and $\nu_{sy}(CO_2^-)$ in the IR spectrum has been successfully used to derive information regarding bonding modes of carboxylic groups.[11a,b] In general, if $\Delta\nu$ is larger than 200 cm^{-1}, carboxylic groups employ the monodentate coordination mode; in contrast, if $\Delta\nu$ is smaller than 200 cm^{-1}, carboxylic groups utilize the chelating coordination fashion.[11c] Thus, the $\Delta\nu$ of 246 cm^{-1} for **1** shows the monodentate coordination mode of the carboxylic groups in **1**, while the $\Delta\nu$ of 200 cm^{-1} for **2** may indicate the coexistence of monodentate and chelating coordination mode of the carboxylic groups in **2**. These results are consistent with their crystal structures. The broadened vibration bands centered at 3457 cm^{-1} in **1** and 3433 in **2** are indicative of the presence of lattice

water molecules. In short, the results of IR spectra are in good agreement with X-ray single-crystal structural analyses.

Structure Description. X-ray single-crystal structural analysis indicates that **1** crystallizes in the triclinic space group $P\bar{1}$. The structural unit of **1** consists of one lantern-shaped $[(CuO_6)Mo_6O_{18}(As_3O_3)_2]^{4-}$ polyoxoanion (POA), two $[Cu(arg)_2]^{2+}$ cations, and four lattice water molecules (Figure 1a).
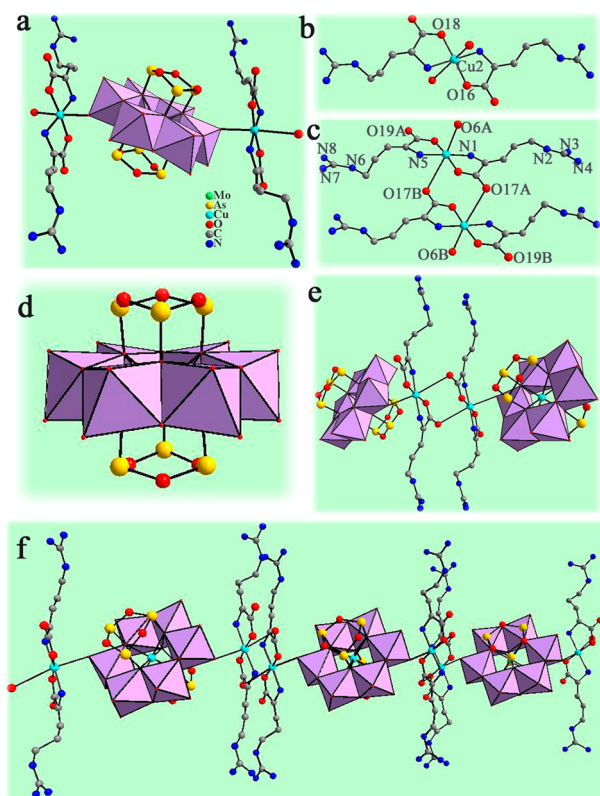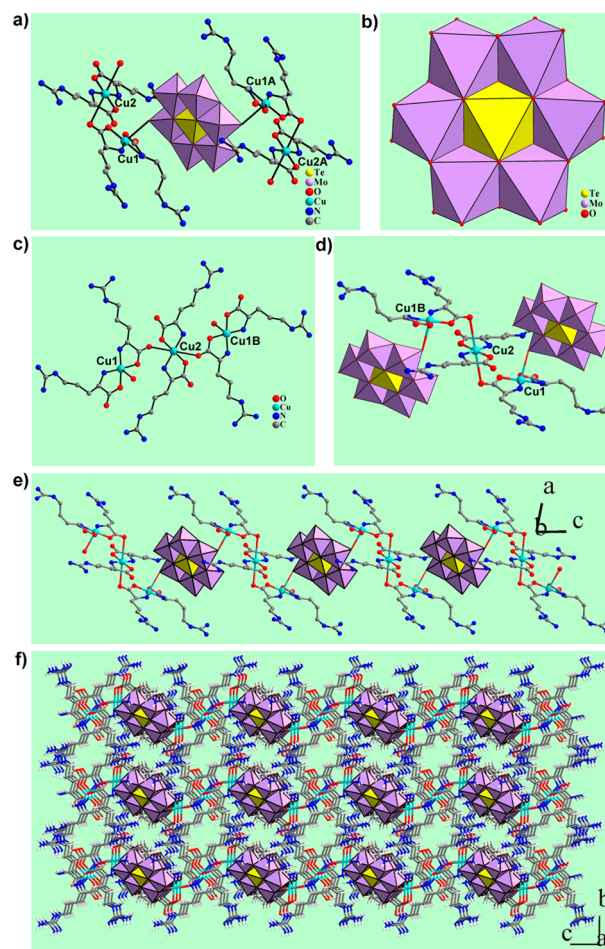

Figure 1. (a) Ball-and-stick/polyhedral representation of the structural unit of **1** with the selected labeling scheme. Lattice water molecules and hydrogen atoms are omitted for clarity. (b) The coordination environment of $[Cu(arg)_2]^{2+}$ cation. (c) Connection of neighboring two $[Cu(arg)_2]^{2+}$ cations forming a novel dinuclear $[Cu(arg)_2]_2^{4+}$ cation. (d) Ball-and-stick/polyhedral view of the $[(CuO_6)$-$Mo_6O_{18}(As_3O_3)_2]^{4-}$ POA. (e) Combination of adjacent two structural units. (f) 1D chain structure of **1**. The atoms with the suffixes A and B are generated by the symmetry operation. A: x, $-1 + y$, $-1 + z$; B: $1 - x$, $1 - y$, $-z$.

Bond valence sum calculations show that the oxidation states of the Mo, As, and Cu atoms are +6, +3, and +2, respectively,[12] which are in good agreement with their coordination geometries. Obviously, the As_2O_3 reactant was not oxidized in the formation process of **1** at the 110 °C hydrothermal reaction, which well abides by the conclusion made by our laboratory: when the reaction temperature is higher than 150 °C, the As[III] atoms are oxidized to the As[V] atoms entirely and when the reaction temperature is set near 130 °C, the As[III] atoms are partially oxidized, which results in the coexistence of the As[III] and As[V] atoms in the arsenomolybdate fragments; and when the reaction temperature further decreases below 130 °C, the As[III] atoms can be maintained in the arsenomolybdate fragments.[3i] Since there exists the octahedral geometries of the Cu[II] ions in **1**, the evident Jahn–Teller effect occurs and leads to elongation of the Cu–O distances in the crystal field,[7a,13] therefore, the Cu–O weak interactions will be considered in the structural description. In **1**,

there are two crystallographically independent copper ions (Cu1 and Cu2): the Cu1 ion is incorporated in the center of the $[(CuO_6)Mo_6O_{18}(As_3O_3)_2]^{4-}$ POA, while the Cu2 ion exists in the form of the $[Cu(arg)_2]^{2+}$ complex cation. Notably, two $[Cu(arg)_2]^{2+}$ cations are twinned toward each other and situated at either side of the POA by coordination to the terminal oxygen atoms of the POA, which cannot be found in the Cambridge Crystallographic Data Center. Although two crystallographically unique copper ions exhibit the octahedral geometries, their coordination environments are different. The Cu1 cation is surrounded by six μ_4-O atoms in the form of the $\{CuO_6\}$ mode with Cu–O distances of 2.017(7)−2.117(7) Å (Figure 1a), whereas the $[Cu2(arg)_2]^{2+}$ cation is defined by two N atoms from the chelating arg ligands with Cu–N bond lengths of 1.9819(2)−1.9968(2) Å, two carboxyl O atoms from the chelating arg ligands with Cu–O bond lengths of 1.911(8)− 1.926(7) Å, and two terminal O atoms from the POAs [Cu–O: 2.4192(2)−3.1127(4) Å] (Figure 1b). Interestingly, by means of the Cu–O weak interactions, two adjacent $[Cu2(arg)_2]^{2+}$ cations are further combined, giving rise to a novel dinuclear $[Cu(arg)_2]_2^{4+}$ cation with the aid of two μ_3-η^1:η^1:η^1 tridentate arg ligands (Figure 1c). To the best of our knowledge, such a structural connection motif employed in **1** has been rarely reported. It should be pointed out that the novel dinuclear $[Cu(arg)_2]_2^{4+}$ cation provides the indispensable precondition for the construction of the 1D chain architecture. The lantern-shaped $[(CuO_6)Mo_6O_{18}(As_3O_3)_2]^{4-}$ POA (Figure 1d) is derived from the A-type Anderson $[(CuO_6)Mo_6O_{18}]^{10-}$ POA, which is capped by a cyclic As_3O_6 group on each side. In the lantern-shaped POA, the central CuO_6 octahedron is surrounded by six planar in turn joined MoO_6 octahedra in the hexagonally arranged fashion by the edge-sharing mode. The cyclic As_3O_6 trimers cap on the opposite faces of an Anderson-type anion. Each As_3O_6 group consists of three AsO_3 pyramids linked in a triangular arrangement by sharing corners and bonded to the central CuO_6 octahedron and two MoO_6 octahedra via μ_3-oxo groups. The Mo–O and As–O distances are in the range of 1.688(8)−2.352(7) Å and 1.772(8)−1.796(7) Å, respectively. As a matter of fact, this lantern-shaped bis(As_3O_3)-capped Anderson-type arsenomolybdate is first discovered by Jeannin et al.,[14] where a Co-centered arsenomolybdate $[Co(H_2O)_6]$ $K_2[As_6CoMo_6O_{30}]$ was isolated by reaction of $[Co(H_2O)_6]Cl_2$, $Na_3[As_3Mo_3O_{15}]\cdot10H_2O$, and KCl in aqueous solution at room temperature. Since then, some functionalized bis(As_3O_3)-capped M-centered (M = Co, Mo, Cu, Zn, and Ni) Anderson-type arsenomolybdate derivatives are consecutively reported.[3k,h,i,15] In comparison with the previously reported organic−inorganic hybrid bis(As_3O_3)-capped, Cu-centered Anderson-type arsen-omolybdates $(H_2en)[Cu(en)_2][(CuO_6)Mo_6O_{18}(As_3O_3)_2]\cdot$ $10H_2O$ (**A**),[3i] $[Cu(imi)_2]_2[(CuO_6)(As_3O_3)_2Mo_6O_{18}]$ $[Cu$-$(imi)_2]_2$ (**B**),[15d] and $(C_5H_5NH)_2(H_3O)_2[(CuO_6)$-$Mo_6O_{18}(As_3O_3)_2]$ (**C**),[15a] their common characteristic is that they all were prepared under hydrothermal conditions by making use of the same copper source of $CuCl_2\cdot2H_2O$; however, four evident discrepancies between them are also observed. (a) Their arsenic and molybdenum sources are different: As_2O_3 and $(NH_4)_6Mo_7O_{24}\cdot4H_2O$ for **1** and **A**, $NaAsO_2$ and $(NH_4)_6Mo_7O_{24}\cdot4H_2O$ for **B**, $NaAsO_2$ and $Na_2MoO_4\cdot2H_2O$ for **C**. (b) The types of organic components are various: the N,O-containing aminoacid ligand (arg) was used in **1**. Moreover, the N and O atoms simultaneously coordinate to the copper cations, while the N-containing ligands (ethylenediamine, imidazole, and pyridine) were employed in **A**−**C**, and the N atoms in **A** and **B**

bind to the copper cations. On the contrary, the N-containing ligand in **C** is discrete. (c) Their reaction temperatures are distinct: 120 °C for **1**, 130 °C for **A**, 140 °C for **B**, and 170 °C for **C**. (d) **1** displays the 1D chain alignment, while **A**−**C** exhibit the discrete structure. As far as we know, **1** represents the first 1D organic−inorganic hybrid chain constructed from lantern-shaped arsenomolybdate $[(CuO_6)Mo_6O_{18}(As_3O_3)_2]^{4-}$ units and dinuclear copper−arg complexes, albeit some polyoxomolybdates with aminoacid ligands such as $[Mo_8O_{26}(L-lysH_2)_2]^{2-}$,[16a] $[Mo_{154}O_{462}H_{14}(H_2O)_{48}(HO_2C-(NH_3^+)HC-CH_2-S-S-CH_2-CH(NH_3^+)-COO^-)_{11}]^{3-}$,[16b] and $[XMo_6O_{21}(O_2CRNH_3)_3]^{n-}$ ($n = 2$, $X = Se^{IV}$, Te^{IV}; $n = 3$, $X = As^{III}$, Sb^{III}, Bi^{III}; $R = CH_2$, C_2H_4, C_3H_6, $CHCH_3$, and $CH(CH_2)_4NH_2)^{4b}$ have already been reported. In addition, more intriguingly, a combination of adjacent structural units results in the 1D chain structure of **1** (Figure 1, panels e and f). 1D chains are packed into the 3D supramolecular structure via hydrogen-bonding interactions between arg groups and POAs/lattice waters [N−H···O: 2.8438(12) −3.19(3) Å] (Table S1 and Figure S2 of the Supporting Information).

Compound **2** also crystallizes in the triclinic space group $P\bar{1}$, and its molecular structural unit is composed of a typical A-type Anderson-type $[TeMo_6O_{24}]^{6-}$ POA, three $[Cu(arg)_2]^{2+}$ cations, and eight lattice water molecules (Figure 2a). The $[TeMo_6O_{24}]^{6-}$ POA belongs to the A-type Anderson structure with a D_{3d} symmetry, which consists of seven edge-sharing octahedra, in which six $\{MoO_6\}$ octahedra are arranged hexagonally around the central $\{TeO_6\}$ octahedron (Figure 2b). The six molybdenum atoms form a slightly distorted hexagon with the Mo···Mo distances of 3.2687(6)−3.2771(6) Å. The Te^{VI} atom is octahedrally surrounded by six μ_3-oxygen atoms. The Mo−O and Te−O bond lengths are in the range of 1.711(3)−2.299(3) Å and 1.922(3)−1.931(3) Å, respectively, which are similar to those reported in other telluromolybdates.[17] In **2**, there are two crystallographically unique copper ions (Cu1 and Cu2). The $[Cu1(arg)_2]^{2+}$ cation occupies the usual site with a site occupancy factor of 1 and adopts the square pyramid geometry defined by two N atoms and two carboxyl O atoms from two arg ligands [Cu−N: 1.951(5)−1.955(4) Å, Cu−O: 1.941(4)−1.923(4) Å] and one terminal O atom from the $[TeMo_6O_{24}]^{6-}$ POA [Cu−O: 2.744(2) Å], whereas the $[Cu2(arg)_2]^{2+}$ cation is situated on the special position (0, 1, 0) with the site occupancy factor of 0.5 and displays the octahedral geometry, in which two N atoms and two carboxyl O atoms from two arg ligands build the basal plane [Cu−N: 1.977(4) Å; Cu−O: 1.922(4) Å] and two carboxyl O atoms from two other arg ligands occupy two axial positions [Cu−O: 3.134(3) Å]. The most remarkable characteristic is that the neighboring two $[Cu1(arg)_2]^{2+}$ cations can be linked together by the $[Cu2(arg)_2]^{2+}$ connector, considering the Cu−O weak bonds derived from the Jahn−Teller distortion of the Cu^{2+} cation in the ligand field. Thus, a particular trinuclear $[Cu_3(arg)_6]^{6+}$ linkage comes into being (Figure 2, panels c and d). It is striking that the tridentate arg ligand plays an important role in the construction of this trinuclear $[Cu_3(arg)_6]^{6+}$ linkage. In the help of this trinuclear $[Cu_3(arg)_6]^{6+}$ linkage, the unprecedented 1D polymeric chain is assembled (Figure 2e), which is completely distinct from that 1D open racklike architecture $[\{Na_4(H_2O)_{14}\}-\{Cu(gly)\}_2][TeMo_6O_{24}]$ (**D**).[4a] The major discrepancies **2** and **D** lie in two aspects: (i) **2** was made by K_2TeO_3, $CuCl_2·2H_2O$, $(NH_4)_6Mo_7O_{24}·4 H_2O$, and arg under 110 °C hydrothermal conditions, and in contrast, **D** was prepared by H_6TeO_6, $Na_2MoO_4·2H_2O$, $CuCl_2·2H_2O$, and glycine in conventional

Figure 2. (a) Ball-and-stick/polyhedral representation of the structural unit of **2** with the selected numbering scheme. Lattice water molecules and hydrogen atoms are omitted for clarity. (b) Polyhedral view of the Anderson-type $[TeMo_6O_{24}]^{6-}$ POA. (c) Connection of neighboring three $[Cu(arg)_2]^{2+}$ cations constructing a particular trinuclear $[Cu_3(arg)_6]^{6+}$ cation. (e) Combination of two $[TeMo_6O_{24}]^{6-}$ POAs and a trinuclear $[Cu_3(arg)_6]^{6+}$ linker. (f) 1D polymeric chain of **2**. The atoms with the suffixes A and B are generated by the symmetry operation. A: −x, 2 − y, 1 − z; B: −x, 2 − y, −z.

aqueous solution. (ii) The 1D chain in **2** is constructed from Anderson $[TeMo_6O_{24}]^{6-}$ POAs via trinuclear $[Cu_3(arg)_6]^{6+}$ linkages, whereas the 1D open racklike architecture in D is based on Anderson $[TeMo_6O_{24}]^{6-}$ POAs as steps and cationic Cu−organic complexes as handles of the rack. As far as we know, **2** represents the second organic− inorganic hybrid 1D chain telluromolybdate with TM−aminoacid complexes. Similar to **1**, in **2** arg ligands on copper cations act as the proton donors, surface oxygen atoms of $[TeMo_6O_{24}]^{6-}$ POAs, oxygen and nitrogen atoms of arg ligands and lattice water molecules work as the proton acceptors, thus donors and acceptors are hydrogen-bonded together generating the infinitely 3-D extended supramolecular framework with O−H···O, O−H···N, N−H···O and N−H···N distances of 2.816(9)Å, 2.721(6) −2.784(7) Å, 2.721(6)−3.317(7) Å and 3.296(10) Å, respectively (Figure 2f, Table S2, Supporting Information).

Magnetic Properties. In accordance with the structural feature described above, **1** and **2** contain dinuclear $[Cu(arg)_2]_2^{4+}$ clusters and trinuclear $[Cu(arg)_2]_3^{6+}$ clusters, respectively, bridged by arg ligands, therefore their magnetic behaviors are studied in the range from 2 to 300 K and the plots of χ_M, $\chi_M T$, and

1471

dx.doi.org/10.1021/cg500019g | *Cryst. Growth Des.* 2014, 14, 1467−1475

χ_M^{-1} versus T are shown in Figure 3. The χ_M value slowly increases from 0.004 emu mol^{-1} for **1** and 0.004 emu mol^{-1} for **2** at 300 K to 0.065 emu mol^{-1} for **1** and 0.061 emu mol^{-1} for **2** at 20 K and then exponentially to the maximum of 0.619 emu mol^{-1} for **1** and 0.595 emu mol^{-1} for **2** at 2 K (Figure 3, panels a and c). Correspondingly, the $\chi_M T$ value corresponds to 1.30 emu mol^{-1} K for **1** and 1.23 emu mol^{-1} K for **2** at 300 K, which is in good consistence with the spin-only contribution (1.24 emu mol^{-1} K) expected for three noninteracting Cu^{II} atoms, considering $g = 2.1$ per formula unit. When the system is cooled from 300 K to approximately 24 K for **1** and from 300 K to approximately 50 K for **2**, the $\chi_M T$ product is approximately a constant with a slight decrease. Below 24 K for **1** and 50 K for **2**, the $\chi_M T$ product decreases with further decreasing temperatures, reaching the minimum of 1.24 emu mol^{-1} K for **1** and 1.19 emu mol^{-1} K for **2** at 2 K. This behavior indicates the very weak antiferromagnetic interactions within dinuclear $[Cu(arg)_2]_2^{4+}$ cations for **1** and trinuclear $[Cu(arg)_2]_3^{6+}$ clusters for **2**. The temperature dependence of the reciprocal susceptibility data is well-fitted by the Curie–Weiss expression with $C = 1.30$ emu mol^{-1} K and $\theta = -0.10$ K for **1** and $C = 1.23$ emu mol^{-1} K and $\theta = -0.13$ K for **2** (Figure 3, panels b and d). The small negative Weiss constant consolidates the presence of weak antiferromagnetic coupling within copper centers, which also coincides with the case that the copper centers in dinuclear $[Cu(arg)_2]_2^{4+}$ cations for **1** and trinuclear $[Cu(arg)_2]_3^{6+}$ clusters for **2** are magnetically mediated by the carboxyl groups of arg ligands. In order to quantitatively evaluate the magnetic coupling interactions within dinuclear $[Cu(arg)_2]_2^{4+}$ cations for **1**, the magnetic susceptibility data are fitted by the Bleaney–Bowers equation[18] and the contribution of a mononuclear Cu^{2+} ion using the expression 1:

$$\chi_M = \frac{2Ng^2\beta^2}{kT} \times \frac{1}{3 + e^{-2J/kT}} + \frac{Ng^2\beta^2}{3kT}s(s+1) \quad (1)$$

where J is the exchange constant between dinuclear $[Cu(arg)_2]_2^{4+}$ cation, s is the spin value of one Cu^{2+} ion and N, g, and β parameters have their usual meaning. The fitting parameters are $J = -2.777$ cm^{-1} and $g = 2.153$, which further confirms the weak antiferromagnetic coupling interactions within dinuclear $[Cu(arg)_2]_2^{4+}$ cations for **1**. Similarly, the magnetic behavior of **2** can be approximately simulated by the linear {Cu$_3$} model:

$$\underset{S_2}{A} \overset{J}{\rule{2cm}{0.4pt}} \underset{S_1}{B} \overset{J}{\rule{2cm}{0.4pt}} \underset{S_3}{A}$$
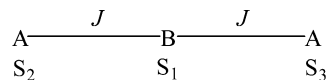
where A represents the Cu1 and Cu1B cations and B stands for the Cu2 cation (Figure 2c). The magnetic susceptibility data can be fitted by the expression 2:

$$\chi_M = \frac{Ng^2\beta^2}{4kT} \times \frac{1 + e^{2J/kT} + 10e^{3J/kT}}{1 + e^{2J/kT} + 2e^{3J/kT}} \quad (2)$$

where J is the exchange constant in the trinuclear $[Cu(arg)_2]_3^{6+}$ clusters for **2**. A good agreement with the experimental data is obtained with the following parameters of $J = -0.195$ cm^{-1} and $g = 2.092$, which proves the weak antiferromagnetic coupling among the trinuclear $[Cu(arg)_2]_3^{6+}$ clusters. As a matter of fact, the antiferromagnetic exchange interactions of the multicopper-substituted POMs have been already been encountered in the previous reports, such as $[Na_{12}(H_2O)_{36}][Cu_2(\beta\text{-}Y\text{-}GeMo_9O_{33})_2]\cdot 3H_2O,$[19a] $K_{10}[Cu_5(OH)_4(H_2O)_2(A\text{-}\alpha\text{-}SiW_9O_{33})_2]\cdot 18.5H_2O,$[19b] $[\{Cu_6(\mu_3\text{-}OH)_3(en)_3(H_2O)_3\}(B\text{-}\alpha\text{-}PW_9O_{34})]\cdot 7H_2O,$[19c] and $[Cu^{II}_2(H_2O)_2(2,2'\text{-}bpy)_2]$-
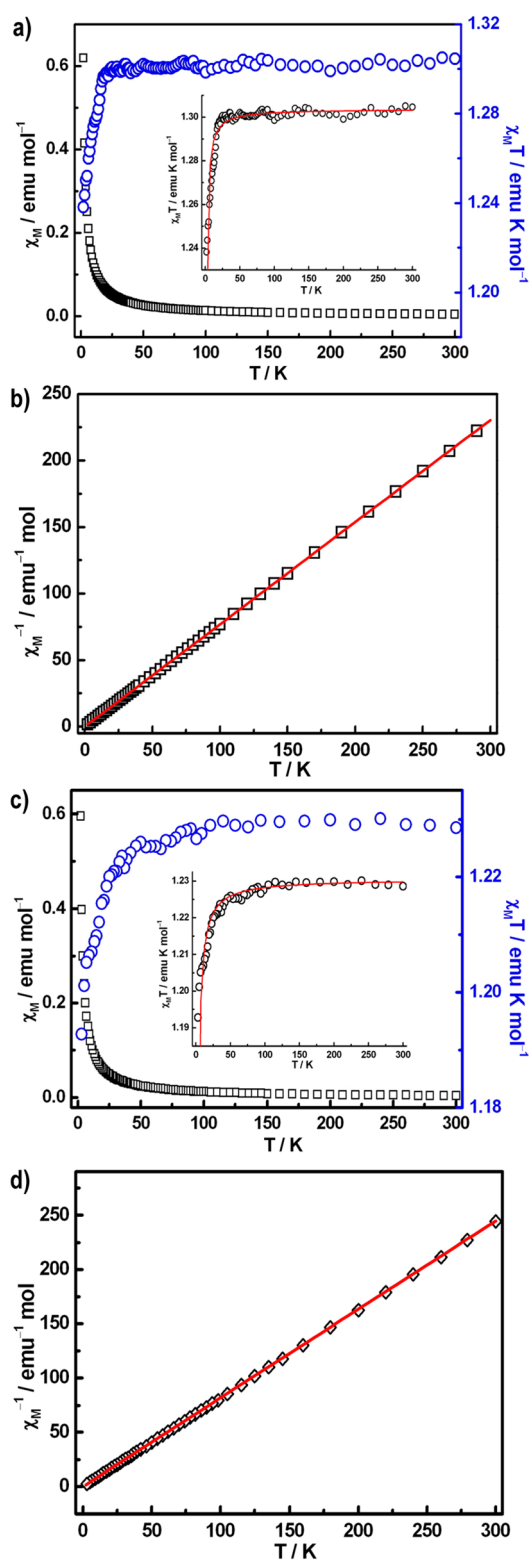
Figure 3. (a) Temperature dependence of magnetic susceptibility for **1** between 2 and 300 K. The inset illustrates the fitting of $\chi_M T$ versus T. (b) Temperature evolution of the inverse magnetic susceptibility for **1** between 2 and 300 K. (c) Temperature dependence of magnetic susceptibility for **2** between 2 and 300 K. The inset illustrates the fitting of $\chi_M T$ versus T. (d) Temperature evolution of the inverse magnetic susceptibility for **2** between 2 and 300 K. The red solid lines in b and d were generated from the best fit by the Curie–Weiss expression.

$\{[Cu^{II}(bdyl)]_2[Cu^{II}_8(2,2'\text{-bpy})_4(H_2O)_2(B\text{-}\alpha\text{-}GeW_9O_{34})_2]\}\cdot 4H_2O.$[19d]
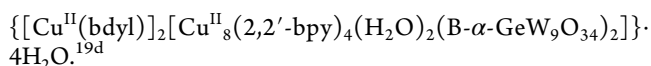
Electrochemical and Electrocatalytic Properties. The ability of POMs undergoing reversible multielectron redox processes makes them very attractive in the chemically modified electrode and electrocatalytic study.[20] The electrochemical behavior of **1** was measured. Because **1** is hydrothermally obtained and has poor solubility in aqueous solution, **1** can be used as the modified carbon paste electrode (**1**-CPE) to investigate the electrochemical behavior and electrocatalytic activities. The cyclic voltammogram for **1**-CPE in 1 mol L^{-1} H$_2$SO$_4$ aqueous solution at a scan rate of 50 mV s^{-1} is shown in Figure 4a. It can be seen that in the potential range of −200 to 800 mV, three quasi-reversible redox peaks with the mean peak potentials $E_{1/2} = (E_{pa} + E_{pc})/2$ are 430 (I−I'), 313 (II−II'), and 126 (III−IIII') mV, respectively, and an irreversible anodic peak (IIII) at +126 mV (vs the Ag/AgCl electrode) are observed. The redox peaks (I−I', II−II', and III−III') may correspond to the redox processes for the Mo centers,[15d,21] while the irreversible anodic peak (IIII) should be assigned to the oxidation of the copper centers.[19b,22] The peak potential separations of the Mo-based wave are around 132 mV for I−I', 128 mV for II−II', and 197 mV for III−III', which correspond to a semireversible one-electron charge-transfer process. Moreover, the influence of the scan rate on electrochemical behavior of **1**-CPE has been probed in the potential range of −200 to 800 mV in the above-mentioned conditions. Figure 4b illustrates the variation of the anodic peak current of the redox peak (II−II') of the Mo-based wave with the scan rate. When the scan rate is varied from 20 to 110 mV s^{-1}, the peak current intensity (I_{pa}) is proportional to the scan rate (v), and its linear equation is $I_{pa} = 1.437 \times 10^{-8} v + 3.217 \times 10^{-7}$ with the correlation coefficient of 0.988, which suggests a surface-controlled electron transfer process occurring at **1**-CPE.[23] POMs have been extensively exploited in electrocatalytic reduction in the past several years due to their ability to undergo reversible multielectron redox processes.[20,24] For instance, Nohra and co-workers observed the high electrocatalytic efficiency for the hydrogen evolution reaction of POM-based framework materials (TBA)$_3$[P Mo$^V_8$Mo$^{VI}_4$O$_{36}$(OH)$_4$Zn$_4$]-[C$_6$H$_3$(COO)$_3$]$_{4/3}$·6H$_2$O, (TBA)$_3$[PMo$^V_8$Mo$^{VI}_4$O$_{37}$(OH)$_3$Zn$_4$][C$_6$H$_3$(COO)$_3$], and (TBA)$_3$[PMo$^V_8$Mo$^{VI}_4$O$_{37}$(OH)$_3$Zn$_4$][C$_6$H$_3$(COO)$_3$]·8H$_2$O.[23a] The electrocatalytic activities of (pbpy)$_4$H[PMo$_{12}$O$_{40}$(VO)]-CPE and (pbpy)$_4$H$_4$[SiMo$_{12}$O$_{40}$]-CPE for the reduction of chlorate were investigated by Peng et al.[20] Herein, we respectively probed the electrocatalytic activities of **1**-CPE toward the reduction of nitrite and bromate in 1 mol L^{-1} H$_2$SO$_4$ aqueous media at the scan rate of 50 mV s^{-1}. As is well-known, nitrite is a common pollutant from agricultural and industrial sources. Its direct electroreduction requires a large overpotential at most electrode surfaces and no response is observed in the range of −200 to 800 mV at a bare CPE in a solution containing NO$_2^-$.[25] Dong and Keita et al. have reported the electrocatalytic reduction of NO$_2^-$ with [SiW$_{12}$O$_{40}$]$^{4-}$ and POMs/polymer system, respectively.[26] Figure 4c shows the cyclic voltammograms for the electrocatalytic reduction of nitrite by **1**-CPE in 1 mol L^{-1} H$_2$SO$_4$ aqueous solution. It can be seen that with the addition of nitrite, all of the reduction peak currents increase gradually, while the corresponding oxidation peak currents decrease, which indicates that the reduction of nitrite is simultaneously mediated by the Cu-based wave and the Mo-based waves. The phenomenon shows that **1**-CPE displays obvious electrocatalytic activity toward the reduction of nitrite.
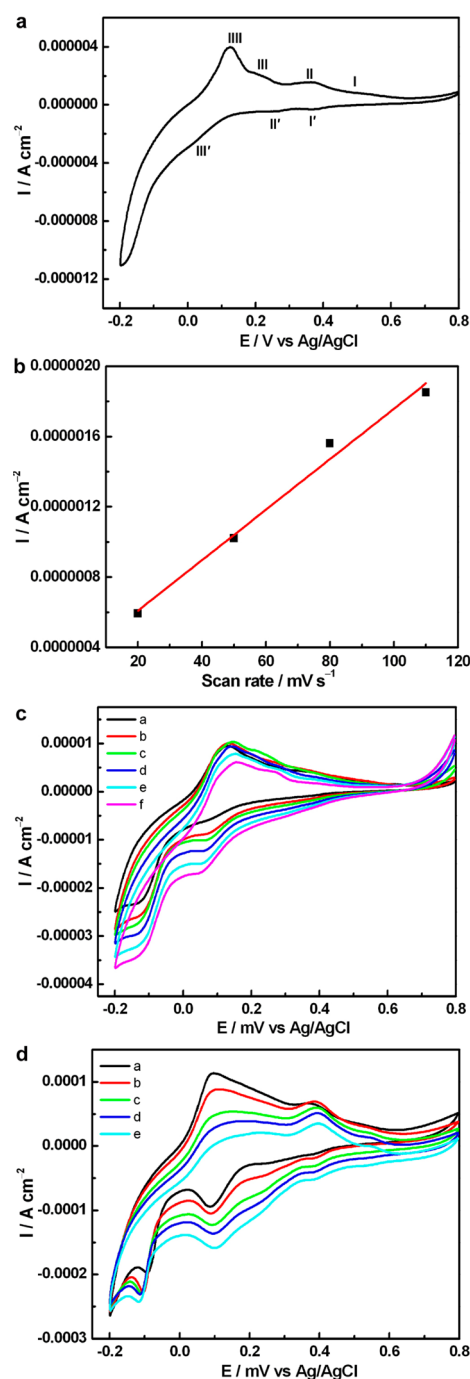
Figure 4. (a) Cyclic voltammogram of 1-CPE in 1 mol L^{-1} H$_2$SO$_4$ aqueous solution. (b) Variation of anodic peak current of the Mo-based wave with the scan rate for 1-CPE. (c) Cyclic voltammograms of 1-CPE in 1 mol L^{-1} H$_2$SO$_4$ aqueous solution containing various concentrations (a, 1×10^{-3}; b, 3×10^{-3}; c, 5×10^{-3}; d, 7×10^{-3}; e, 9×10^{-3}; and f, 1.1×10^{-2} mol L^{-1}) of NaNO$_2$. (d) Cyclic voltammograms of 1-CPE in 1 mol L^{-1} H$_2$SO$_4$ aqueous solution containing various concentrations (a, 1×10^{-3}; b, 3×10^{-3}; c, 5×10^{-3}; d, 7×10^{-3}; and e, 9×10^{-3} mol L^{-1}) of NaBrO$_3$. Scan rate is 50 mV s^{-1}.

As we know, bromate is suspected to act as a human carcinogen,[27] therefore, the monitoring or removal of this species is of interest as it is present in drinking water samples as a byproduct of ozone disinfection and is often used as a food additive.[28] Generally, the reduction of bromate is totally irreversible at a glassy carbon electrode in acidic aqueous

solution and does not take place prior to the evolution of hydrogen.[29] Experiments have attested that the reduction of bromate can readily be catalyzed by the mixed valence molybdenum or tungsten species.[30] In order to check the electrocatalytic potential of **1**-CPE toward the reduction of bromate, cyclic voltammetry measurements of **1**-CPE in 1 mol L^{-1} H_2SO_4 aqueous solution containing various concentrations of $NaBrO_3$ have also been performed at room temperature. Figure 4d exhibits the cyclic voltammograms for the electrocatalytic reduction of $NaBrO_3$ by **1**-CPE. With addition of bromate, the reduction peak currents of the Cu-based wave are less affected, whereas the reduction peak currents of the Mo-based wave increase gradually and the corresponding oxidation peak currents decrease gradually. The result manifests that the reduction of bromate is mainly mediated by the reduced species of Mo-oxo cluster in **1**, which is somewhat different from the reduction of nitrite that is simultaneously mediated by the Cu-based wave and the Mo-based waves. In addition, since $(NH_4)_6Mo_7O_{24}\cdot4H_2O$ was used as a starting material in the preparation of **1**, to probe whether it has the electrocatalytic activities toward the nitrite and bromate reduction, relevant electrocatalytic measurements of $(NH_4)_6Mo_7O_{24}\cdot4H_2O$ have been performed in 1 mol L^{-1} H_2SO_4 aqueous solution under ambient conditions using the three electrode assembly consisting of a 4 mm diameter glassy carbon disk electrode (GCE) as the working electrode, Ag/AgCl as the reference electrode, and a platinum wire as the auxiliary (counter) electrode. As shown in Figure S4 of the Supporting Information, the cyclic voltammogram of $(NH_4)_6Mo_7O_{24}\cdot4H_2O$ in 1 mol L^{-1} H_2SO_4 aqueous solution is characterized by two ill-defined reductive signals at $E_{1/2}$ = 429 mV (I–I′) and 31.5 mV (II–II′), due to reduction of the molybdenum cluster. With the addition of $NaNO_2$ or $NaBrO_3$ (Figures S5 and S6 of the Supporting Information), all of the reduction peak currents very tardily increase and the corresponding oxidation peak currents very slowly decrease, which illustrate that $(NH_4)_6Mo_7O_{24}\cdot4H_2O$ has quite weak electrocatalytic activity toward the reduction of nitrite and bromate. In other words, the above results indicate that **1**-CPE has obvious electrocatalytic activities toward the nitrite and bromate reduction, which may be important for practical applications.

CONCLUSIONS

In summary, two novel organic−inorganic hybrid HPMs **1** and **2** with copper−aminoacid complexes have been hydrothermally synthesized and structurally characterized. **1** is the first 1D chain organic−inorganic hybrid arsenomolybdate constructed from lantern-shaped $[(CuO_6)Mo_6O_{18}(As_3O_3)_2]^{4-}$ units via dinuclear $[Cu_2(arg)_4]^{4+}$ bridges, while **2** is an unseen 1D chain organic−inorganic hybrid telluromolybdate built by Anderson-type $[TeMo_6O_{24}]^{6-}$ fragments by trinuclear $[Cu_3(arg)_6]^{6+}$ linkers. The magnetic susceptibility measurements of **1** and **2** display the weak antiferromagnetic coupling within copper centers mediated by the carboxyl groups of arg ligands. The solid-state electrochemical and electrocatalytic properties of **1** have been carried out in 1 mol L^{-1} H_2SO_4 aqueous solution by entrapping it in a carbon paste electrode. The results indicate that **1**-CPE has apparent electrocatalytic activities toward the reduction of nitrite and bromate. This work further confirms that aminoacid ligands can be introduced to the HPM/TM system by the low-temperature hydrothermal technique, which endows us with great opportunity and challenge in exploiting and making novel organic−inorganic hybrid HPM-based derivatives with amino-

acid ligands. In the following work, different amino acids and TM cations will be used in the reaction system to construct much more HPM-based hybrids with aminoacid ligands. This work is in progress.

ASSOCIATED CONTENT

Ⓢ Supporting Information

IR spectra of **1** and **2**, the structure of L-arginine, the 3D supramolecular structure of **2**, hydrogen-bonding information of **1** and **2**, thermogravimetri analyses of **1** and **2**, the electrocatalytic properties of $(NH_4)_6Mo_7O_{24}\cdot4H_2O$, and the CIF files of **1** and **2**. This material is available free of charge via the Internet at http://pubs.acs.org.

AUTHOR INFORMATION

Corresponding Authors
*E-mail: zhaojunwei@henu.edu.cn. Fax: (+86) 371 23886876.
*E-mail: ljchen@henu.edu.cn.

Notes
The authors declare no competing financial interest.

REFERENCES

(1) (a) Cadot, E.; Sokolov, M. N.; Fedin, V. P.; Simonnet-Jégat, C.; Floqueta, S.; Sécheresse, F. *Chem. Soc. Rev.* **2012**, *41*, 7335. (b) Banerjee, A.; Bassil, B. S.; Röschenthaler, G.-V.; Kortz, U. *Chem. Soc. Rev.* **2012**, *41*, 7590. (c) Zheng, S. T.; Yang, G. Y. *Chem. Soc. Rev.* **2012**, *41*, 7623. (d) Du, D. Y.; Yan, L. K.; Su, Z. M.; Li, S. L.; Lan, Y. Q.; Wang, E. B. *Coord. Chem. Rev.* **2013**, *257*, 702.

(2) (a) Zhang, Z. M.; Li, Y. G.; Wang, Y. H.; Qi, Y. F.; Wang, E. B. *Inorg. Chem.* **2008**, *47*, 7615. (b) Han, Q. X.; He, C.; Zhao, M.; Qi, B.; Niu, J. Y.; Duan, C. Y. *J. Am. Chem. Soc.* **2013**, *135*, 10186. (c) Ma, F.-J.; Liu, S.-X.; Sun, C.-Y.; Liang, D.-D.; Ren, G.-J.; Wei, F.; Chen, Y.-G.; Su, Z.-M. *J. Am. Chem. Soc.* **2011**, *133*, 4178. (d) Uchida, S.; Kawamoto, R.; Tagami, H.; Nakagawa, Y.; Mizuno, N. *J. Am. Chem. Soc.* **2008**, *130*, 12370. (e) Nohra, B.; Moll, H. E.; Albelo, L. M. R.; Mialane, P.; Marrot, J.; Mellot-Draznieks, C.; O'Keeffe, M.; Biboum, R. N.; Lemaire, J.; Keita, B.; Nadjo, L.; Dolbecq, A. *J. Am. Chem. Soc.* **2011**, *133*, 13363. (f) Xiang, X.; Fielden, J.; Rodríguez-Córdoba, W.; Huang, Z.; Zhang, N.; Luo, Z.; Musaev, D. G.; Lian, T.; Hill, C. L. *J. Phys. Chem. C* **2013**, *117*, 918. (g) Kawamoto, R.; Uchida, S.; Mizuno, N. *J. Am. Chem. Soc.* **2005**, *127*, 10560.

(3) (a) Yu, H.-H.; Cui, X.-B.; Cui, J.-W.; Kong, L.; Duan, W.-J.; Xu, J.-Q.; Wang, T.-G. *Dalton Trans.* **2008**, 195. (b) Han, Q. X.; Ma, P. T.; Zhao, J. W.; Wang, Z. L.; Yang, W. H.; Guo, P. H.; Wang, J. P.; Niu, J. Y. *Cryst. Growth Des.* **2011**, *11*, 436. (c) Liu, C.-M.; Zhang, D.-Q.; Zhu, D.-B. *Cryst. Growth Des.* **2006**, *6*, 524. (d) Lei, C.; Mao, J.-G.; Sun, Y.-Q.; Song, J.-L. *Inorg. Chem.* **2004**, *43*, 1964. (e) Walsh, J.; Zhu, J.; Zeng, Q.; Forster, R. J.; Keyes, T. E. *Dalton Trans.* **2012**, *41*, 9928. (f) Jin, H.-J.; Zhou, B.-B.; Yu, Y.; Zhao, Z.-F.; Su, Z.-H. *CrystEngComm* **2011**, *13*, 585. (g) Zang, H.-Y.; Tan, K.; Guan, W.; Li, S.-L.; Yang, G.-S.; Shao, K.-Z.; Yan, L.-K.; Su, Z.-M. *CrystEngComm* **2010**, *12*, 3684. (h) Sun, C. Y.; Li, Y. G.; Wang, E. B.; Xiao, D. R.; An, H. Y.; Xu, L. *Inorg. Chem.* **2007**, *46*, 1563. (i) Niu, J. Y.; Hua, J. H.; Ma, X.; Wang, J. P. *CrystEngComm* **2012**, *14*, 4060. (j) Shivaiah, V.; Nagaraju, M.; Das, S. K. *Inorg. Chem.* **2003**, *42*,

6604. (k) Li, L.; Liu, B.; Xue, G.; Hu, H.; Fu, F.; Wang, J. *Cryst. Growth Des.* **2009**, *9*, 5206. (l) Liu, B.; Yu, Z.-T.; Yang, J.; Hua, W.; Liu, Y.-Y.; Ma, J.-F. *Inorg. Chem.* **2011**, *50*, 8967.

(4) (a) Dutta, D.; Jana, A. D.; Debnath, M.; Bhaumik, A.; Marek, J.; Ali, M. *Dalton Trans.* **2010**, *39*, 11551. (b) Kortz, U.; Savelieff, M. G.; Abou Ghali, F. Y.; Khalil, L. M.; Maalouf, S. A.; Sinno, D. I. *Angew. Chem., Int. Ed.* **2002**, *41*, 4070. (c) Cindrić, M.; Strukan, N.; DevÁić, M.; Kamenar, B. *Inorg. Chem. Commun.* **1999**, *2*, 558.

(5) (a) Zhao, J. W.; Shi, D. Y.; Chen, L. J.; Ma, P. T.; Wang, J. P.; Niu, J. Y. *CrystEngComm* **2011**, *13*, 3462. (b) Zhao, J. W.; Shi, D. Y.; Chen, L. J.; Cai, X. M.; Wang, Z. Q.; Ma, P. T.; Wang, J. P.; Niu, J. Y. *CrystEngComm* **2012**, *14*, 2797. (c) Zhao, J. W.; Shi, D. Y.; Chen, L. J.; Ma, P. T.; Wang, J. P.; Zhang, J.; Niu, J. Y. *Cryst. Growth Des.* **2013**, *13*, 4368.

(6) Liu, H.; Qin, C.; Wei, Y.-G.; Xu, L.; Gao, G.-G.; Li, F.-Y.; Qu, X.-S. *Inorg. Chem.* **2008**, *47*, 4166.

(7) (a) Li, B.; Zhao, J. W.; Zheng, S. T.; Yang, G. Y. *Inorg. Chem.* **2009**, *48*, 8294. (b) Zhao, J. W.; Shi, D. Y.; Chen, L. J.; Li, Y. Z.; Ma, P. T.; Wang, J. P.; Niu, J. Y. *Dalton Trans.* **2012**, *41*, 10740.

(8) (a) Sheldrick, G. M. *SHELXS 97, Program for Crystal Structure Solution*; University of Göttingen: Göttingen, Germany, 1997. (b) Sheldrick, G. M. *SHELXL 97, Program for Crystal Structure Refinement*; University of Göttingen: Germany, 1997.

(9) (a) Hasenknopf, B.; Delmont, R.; Gouzerh, P. *Eur. J. Inorg. Chem.* **2002**, 1081. (b) Xu, H.; Li, L.; Liu, B.; Xue, G.; Hu, H.; Feng, F.; Wang, J. *Inorg. Chem.* **2009**, *48*, 10275. (c) Li, L.; Shen, Q.; Xue, G.; Xu, H.; Hu, H.; Feng, F.; Wang, J. *Dalton Trans.* **2008**, 5698. (d) Yang, D.; Li, S.; Ma, P.; Wang, J.; Niu, J. *Inorg. Chem.* **2013**, *52*, 8987. (e) Asai, T.; Kiriyama, R. *Bull. Chem. Soc. Jpn.* **1973**, *46*, 2395. (f) Liu, Ying; Li, Y.-X.; Zhang, S.-W.; Ji, H.-M.; Cao, R.-Ge.; Liu, S.-X. *J. Mol. Struct.* **2009**, *921*, 114.

(10) (a) Chen, W. L.; Li, Y. G.; Wang, Y. H.; Wang, E. B.; Su, Z. M. *Dalton Trans.* **2007**, 4293. (b) Szeto, K. C.; Lillerud, K. P.; Tilset, M.; Bjørgen, M.; Prestipino, C.; Zecchina, A.; Lamberti, C.; Bordiga, S. *J. Phys. Chem. B* **2006**, *110*, 21509. (c) Bordiga, S.; Lamberti, C.; Ricchiardi, G.; Regli, L.; Bonino, F.; Damin, A.; Lillerud, K. P.; Bjørgen, M.; Zecchina, A. *Chem. Commun.* **2004**, 2300.

(11) (a) Li, C. H.; Huang, K. L.; Chi, Y. N.; Liu, X.; Han, Z. G.; Shen, L.; Hu, C. W. *Inorg. Chem.* **2009**, *48*, 2010. (b) An, H.; Han, Z.; Xu, T. *Inorg. Chem.* **2010**, *49*, 11403. (c) Nakamoto, K. *Infrared and Raman Spectra of Inorganic and Coordination Compounds*, 3rd Ed.; New York: John Wiley and Sons, 1978.

(12) Brown, I. D.; Altermatt, D. *Acta Crystallogr.* **1985**, *B41*, 244.

(13) (a) Zhao, J. W.; Zheng, S. T.; Yang, G. Y. *J. Solid State Chem.* **2008**, *181*, 2205. (b) Bassil, B. S.; Nellutla, S.; Kortz, U.; Stowe, A. C.; van Tol, J.; Dalal, N. S.; Keita, B.; Nadjo, L. *Inorg. Chem.* **2005**, *44*, 2659.

(14) Martin-Frère, J.; Jeannin, Y.; Robert, F.; Vaissermann, J. *Inorg. Chem.* **1991**, *30*, 3635.

(15) (a) He, Q. L.; Wang, E. B. *Inorg. Chem. Commun.* **1999**, *2*, 399. (b) He, Q.; Wang, E.; Hu, C.; Xu, L.; Xing, Y.; Lin, Y.; Jia, H. *J. Mol. Struct.* **1999**, *484*, 139. (c) He, Q. L.; Wang, E. B. *Inorg. Chim. Acta* **1999**, *295*, 244. (d) Su, F. Y.; Zhou, B. B.; Zhao, Z. F.; Su, Z. H.; Zhu, C. C. *Cryst. Res. Technol.* **2009**, *44*, 447. (e) Wu, Q.; He, J.; Han, Q. X.; Yang, W. H.; Wang, J. P. *Chin. J. Struct. Chem.* **2010**, *29*, 1219. (f) Wu, Q.; Han, Q. X.; Chen, L. J.; Ma, P. T.; Niu, J. Y. *Z. Naturforsch.* **2010**, *65b*, 163.

(16) (a) Inoue, M.; Yamase, T. *Bull. Chem. Soc. Jpn.* **1995**, *68*, 3055. (b) Müller, A.; Das, S. K.; Kuhlmann, C.; Bögge, H.; Schmidtmann, M.; Diemann, E.; Krickemeyer, E.; Hormes, J.; Modrow, H.; Schindler, M. *Chem. Commun.* **2001**, 655.

(17) (a) Bridgeman, A. J.; Cavigliasso, G. *J. Phys. Chem. A* **2003**, *107*, 6613. (b) Liu, Y.; Liu, S. X.; Ji, H. M.; Zhang, S. W.; Cai, L. L.; Cao, R. G. *J. Cluster Sci.* **2009**, *20*, 535.

(18) Koner, S.; Saha, S.; Mallah, T.; Okamoto, K. I. *Inorg. Chem.* **2004**, *43*, 840.

(19) (a) Li, S. Z.; Zhao, J. W.; Ma, P. T.; Du, J.; Niu, J. Y.; Wang, J. P. *Inorg. Chem.* **2009**, *48*, 9819. (b) Nellutla, S.; van Tol, J.; Dalal, N. S.; Bi, L. H.; Kortz, U.; Keita, B.; Nadjo, L.; Khitrov, G. A.; Marshall, A. G. *Inorg. Chem.* **2005**, *44*, 9795. (c) Zhao, J. W.; Jia, H. P.; Zhang, J.; Zheng, S. T.; Yang, G. Y. *Chem.—Eur. J.* **2007**, *13*, 10030. (d) Zhao, J. W.; Wang, C. M.; Zhang, J.; Zheng, S. T.; Yang, G. Y. *Chem.—Eur. J.* **2008**, *14*, 9223.

(20) Han, Z.; Zhao, Y.; Peng, J.; Feng, Y.; Yin, J.; Liu, Q. *Electroanalysis* **2005**, *17*, 1097.

(21) (a) Sha, J. Q.; Peng, J.; Liu, H. S.; Chen, J.; Dong, B. X.; Tian, A. X.; Su, Z. M. *Eur. J. Inorg. Chem.* **2007**, 1268. (b) Sadakane, M.; Steckhan, E. *Chem. Rev.* **1998**, *98*, 219.

(22) Liu, J. Y.; Cheng, L.; Dong, S. J. *Electroanalysis* **2002**, *14*, 569.

(23) (a) Nohra, B.; Moll, H. E.; Albelo, L. M. R.; Mialane, P.; Marrot, J.; Mellot-Draznieks, C.; O'Keeffe, M.; Biboum, R N.; Lemaire, J.; Keita, B.; Nadjo, L.; Dolbecq, A. *J. Am. Chem. Soc.* **2011**, *133*, 13363. (b) Ammam, M.; Easton, E. B. *Electrochim. Acta* **2011**, *56*, 2847.

(24) Toth, J. E.; Anson, F. C. *J. Am. Chem. Soc.* **1989**, *111*, 2444.

(25) Wang, X.; Hu, H.; Tian, A.; Lin, H.; Li, J. *Inorg. Chem.* **2010**, *49*, 10299.

(26) (a) Dong, S.; Xi, X.; Tian, M. *J. Electroanal. Chem.* **1995**, *385*, 227. (b) Keita, B.; Belhouari, A.; Nadjo, L.; Contant, R. *J. Electroanal. Chem.* **1995**, *381*, 243.

(27) (a) Moore, M. M.; Chen, T. *Toxicology* **2006**, *221*, 190. (b) Bonacquisti, T. P. *Toxicology* **2006**, *221*, 145.

(28) Rodriguez-Albelo, L. M.; Ruiz-Salvador, A. R.; Sampieri, A.; Lewis, D. W.; Gómez, A.; Nohra, B.; Mialane, P.; Marrot, J.; Sécheresse, F.; Mellot-Draznieks, C.; Biboum, R. N.; Keita, B.; Nadjo, L.; Dolbecq, A. *J. Am. Chem. Soc.* **2009**, *131*, 16078.

(29) Wang, X.; Wang, E.; Lan, Y.; Hu, C. *Electroanalysis* **2002**, *14*, 1116.

(30) (a) Wang, B.; Dong, S. *J. Electroanal. Chem.* **1994**, *379*, 207. (b) Lahr, S. K.; Finklea, H. O.; Schultz, F. A. *J. Electroanal. Chem. Interfacial Electrochem.* **1984**, *163*, 237.